

A multi-system geochronology in the Ad-3 borehole, Pannonian Basin (Hungary) with implications for dating volcanic rocks by low-temperature thermochronology and for interpretation of (U–Th)/He data

Martin Danišik,¹ László Fodor,² István Dunkl,³ Axel Gerdes,⁴ János Csizmeg,² Mária Hámor-Vidó⁵ and Noreen J. Evans¹

¹Applied Geology, John de Laeter Centre for Isotope Research, The Institute for Geoscience Research (TIGeR), Curtin University of Technology, GPO Box U1987, Perth, WA 6845, Australia; ²MTA-ELTE Geological, Geophysical and Space Science Research Group, Eötvös University, 1117 Budapest, Pázmány P. Sétány 1/C, Hungary; ³Sedimentology and Environmental Geology, Geoscience Centre, University of Göttingen, Goldschmidtstrasse 3, Göttingen D-37077, Germany; ⁴Institute of Geosciences, Johann Wolfgang Goethe University, Altenhöferallee 1, Frankfurt am Main D-60438, Germany; ⁵Geological and Geophysical Institute of Hungary, Budapest Stefánia 14, Budapest 1143, Hungary

ABSTRACT

Independent geochronological and thermal modelling approaches are applied to a biostratigraphically exceptionally well-controlled borehole, Alcsútdoboz-3 (Ad-3), in order to constrain the age of Cenozoic geodynamic events in the western Pannonian Basin and to test the efficacy of the methods for dating volcanic rocks. Apatite fission track and zircon U–Pb data show two volcanic phases of Middle Eocene (43.4–39.0 Ma) and Early Oligocene (32.72 ± 0.15 Ma) age respectively. Apatite (U–Th)/He ages (23.8–14.8 Ma) and independent thermal and subsidence history models reveal a brief period of heating to 55–70 °C at ~17 Ma caused by an

increased heat-flow related to crustal thinning and mantle upwelling. Our results demonstrate that, contrary to common perception, the apatite (U–Th)/He method is likely to record ‘apparent’ or ‘mixed’ ages resulting from subsequent thermal events rather than ‘cooling’ or ‘eruption’ ages directly related to distinct geological events. It follows that a direct conversion of ‘apparent’ or ‘mixed’ (U–Th)/He ages into cooling, exhumation or erosion rates is incorrect.

Terra Nova, 00, 000–000, 2015

Introduction

Volcanic deposits, such as tephra spread over large areas, represent important markers for dating and correlation of geological, palaeoclimatic and archaeological records (Lowe, 2011). The key requirement for using volcanic deposits as chronostratigraphic markers is the determination of their absolute age. Accurate and precise dating of volcanic deposits may, however, pose a challenge for modern geochronology. Many volcanic rocks do not contain material suitable for dating, and the interpretation of analytical results may be ambiguous owing to limitations of the dating methods such as inaccuracies in calibration, flaws in dated materials or open-system behaviour (Chen *et al.*, 1996;

McDougall and Harrison, 1998; Reimer *et al.*, 2009).

Volcanic deposits containing zircon and/or apatite have traditionally been dated by U–Pb, fission track, and, more recently, by (U–Th)/He and U-series dating methods, and many studies have demonstrated that these can provide accurate results (Seward, 1974; Farley *et al.*, 2002; Bachmann *et al.*, 2007; Schmitt *et al.*, 2011). However, when only one method is applied, even seemingly univocal results can lead to the erroneous assignment of eruption ages to volcanic rocks. For instance, since the U–Pb method dates the crystallization age of zircons, a zircon U–Pb age must pre-date eruption and therefore cannot necessarily be interpreted as the eruption age. In fact, the hiatus between the crystallization and eruption can be as long as several million years (Davies *et al.*, 1994; Siebel *et al.*, 2009). In contrast, zircon and apatite fission track and (U–Th)/He methods with closure temperatures of ~240–60 °C (e.g. Wagner and Van den haute,

1992; Brandon *et al.*, 1998; Farley, 2002; Reiners *et al.*, 2004) can, in some cases, date the true eruption age by recording cooling of minerals in the eruption column during their ascent to the surface or shortly after their deposition. Low-temperature thermochronometers are, however, prone to post-depositional reheating, for instance by subsequent eruptions, which can lead to partial or full resetting, and, potentially, to misinterpretation of results.

In this study, we present a case study demonstrating the importance of a multi-chronological approach when dating volcanic deposits. We target a borehole (Alcsútdoboz Ad-3) in the western Pannonian Basin, which contains a biostratigraphically well-dated Upper Eocene–Oligocene sedimentary succession, intercalated with layers of zircon- and apatite-bearing volcanogenic sandstones that provide key isochrons for dating Cenozoic geodynamic events in the region. A multi-methodological approach, including zircon U–Pb, apatite fission track (AFT) and

Correspondence: Dr. Martin Danišik, John de Laeter Centre for Isotope Research, Applied Geology, Curtin University of Technology, GPO Box U1987, Perth, WA 6845, Australia. Tel.: +61 8 9266 7625; E-mail: m.danisik@curtin.edu.au

(U–Th)/He (AHe) dating, thermal maturity data, and subsidence and thermal modelling, was adopted in an attempt to (i) better constrain the provenance and age of these stratigraphic horizons, (ii) reconstruct their thermal history, and (iii) refine the timing of volcanism in the Pannonian realm.

Besides addressing these objectives, we demonstrate that ages measured by low-temperature thermochronometers cannot be interpreted as ‘cooling’ or ‘eruption’ ages even in seemingly simple cases such as the dating of volcanic rocks. Thus, our study has implications not only for the selection of methodologies for dating volcanic rocks, but also for the interpretation of thermochronological data in general.

Geological setting and borehole stratigraphy

The Pannonian basin is located within the Alpine-Carpathian-Dinaridic Orogen (Fig. 1). In the Palaeogene, the area experienced subduction, which was associated with basin formation in the foreland, forearc and retroarc of the Alpine-Carpathian orogenic belt (Fig. 1a; Tari *et al.*, 1993; Kázmér *et al.*, 2003). The Hungarian retroarc basins are composed of simple synforms, combined with local folds, reverse and strike-slip faults (Fodor *et al.*, 1992; Tari *et al.*, 1993; Csontos and Nagymarosy, 1998; Palotai and Csontos, 2010). The retro-arc flexural basin is divided into two major sub-basins – the Transdanubian Palaeogene basin (TPB) in the SW and the North Hungarian Palaeogene basin (NHPB) in the NE – distinguished by the timing of major subsidence (Middle Eocene vs. latest Eocene-Oligocene) and the presence or absence of an Early Oligocene erosional hiatus respectively (Báldi, 1986). Early Miocene dextral slip separated the NHPB and its counterpart, the Slovenian Palaeogene basin (SPB), along the Periadriatic Fault and Mid-Hungarian Fault Zone (Fig. 1a; Csontos and Nagymarosy, 1998; Fodor *et al.*, 1998).

The Pannonian Basin was formed by back-arc extension starting at ~19 Ma (Royden *et al.*, 1983). Several episodes of crustal faulting, belonging to the syn-rift phase, resulted in the

formation of a system of grabens and ridges (Fig. 1b). The Late Miocene post-rift phase was characterized by basin-wide subsidence (Royden *et al.*, 1983). Basin formation was associated with widespread calcalkaline volcanism (19–11 Ma) related to ongoing subduction and crustal extension (Harangi, 2001).

The borehole Alcsútdoboz Ad-3 is located at the western margin of the

NHPB close to its transition to the TPB (Fig. 1a) and also at the margin of a N–S trending syn-rift graben (Fig. 1b). Borehole stratigraphy (Fig. 2) is summarized after Báldi (1986), Nagymarosy (1990) and Hámorné Vidó *et al.* (2008): Permian dolomites at 815.5–870 m are unconformably overlain by a 635 m thick Palaeogene sequence, which spans biostratigraphically well-dated

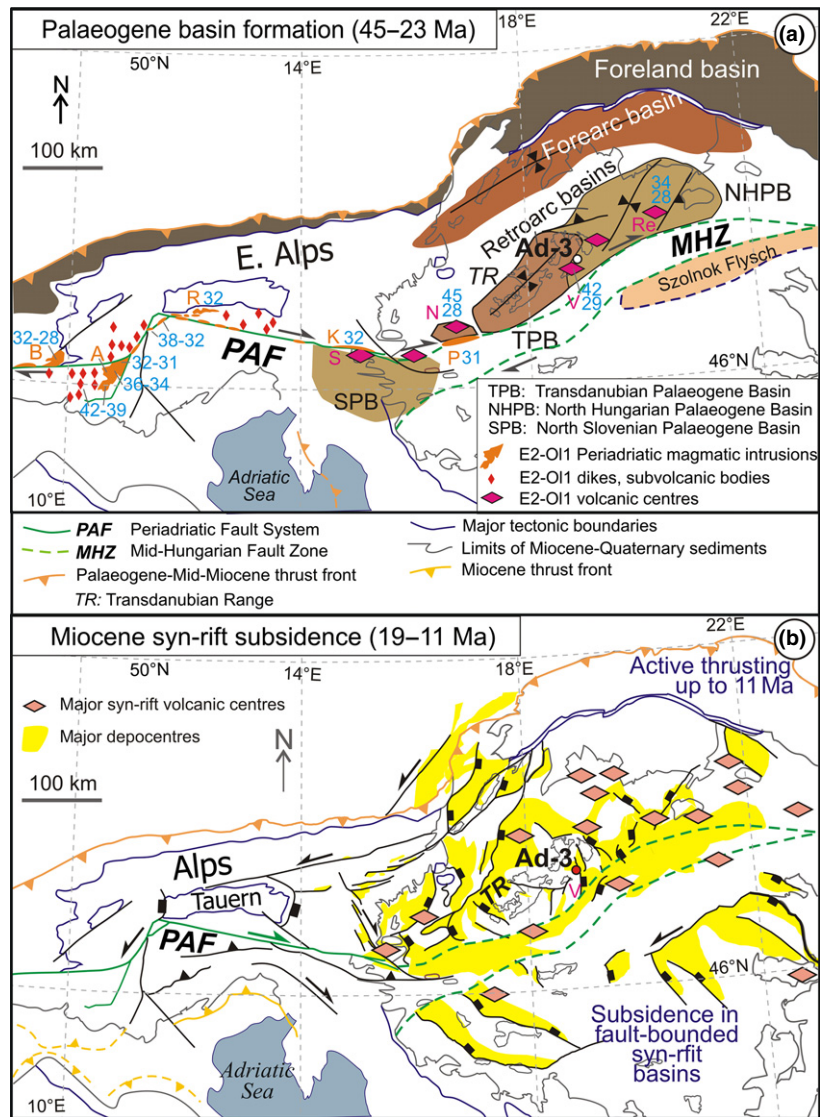


Fig. 1 Simplified tectonic sketch of the Alpine-Carpathian orogens with position of the borehole Ad-3, during the Palaeogene (a) and during the Miocene syn-rift phase (b), modified after Fodor and Kövér (2013). Palaeogene magmatic centres and their ages in Ma after Pomella *et al.* (2011), Bergomi *et al.* (2015) and references therein, Benedek (2002) and Benedek *et al.* (2004). Abbreviations for magmatites; A, Adamello; B, Bergell; K, Karavanka; P, Puszta magyaród; R, Riesenferner; volcanites; N, Nova graben; Re, Recks; S, Smrekovec; V, Velence Hills.

Table 1 U–Pb data for sample AD-3-3 (667 m).

Grain	$^{207}\text{Pb}^*$ (cps)	U^\dagger (p.p.m.)	Pb^\ddagger (p.p.m.)	$\frac{\text{Th}}{\text{U}}^\dagger$	$^{206}\text{Pb}/^{238}\text{U}$ (%)	$\pm 2\sigma$	$\pm 2\sigma$	$\pm 2\sigma$	$\pm 2\sigma$	Rho [¶]	$^{206}\text{Pb}/^{238}\text{U}$	$\pm 2\sigma$	$\pm 2\sigma$			
						(%)	(%)	(%)	(%)			(Ma)	(Ma)			
a1	9354	972	5.7	0.93	b.d.	0.005061	2.4	0.03378	6.0	0.04840	5.5	0.40	32.5	0.8	33.7	2.0
a2	10452	1116	6.4	0.91	0.15	0.005001	2.2	0.03245	7.3	0.04706	7.0	0.30	32.2	0.7	32.4	2.3
a3	12488	1297	8.0	1.26	0.01	0.004998	1.9	0.03193	5.4	0.04634	5.1	0.35	32.1	0.6	31.9	1.7
a4	8006	866	5.0	0.85	0.82	0.005066	2.7	0.03246	6.8	0.04647	6.2	0.40	32.6	0.9	32.4	2.2
a5	9038	950	5.6	1.00	1.02	0.005041	2.0	0.03390	6.7	0.04877	6.4	0.30	32.4	0.6	33.8	2.2
a6	5179	535	3.0	0.63	0.40	0.005057	2.3	0.03369	11	0.04833	11	0.20	32.5	0.7	33.6	3.7
a7	8410	878	5.0	0.67	0.23	0.005104	2.2	0.03252	6.8	0.04621	6.4	0.33	32.8	0.7	32.5	2.2
a8	9985	1059	6.7	0.90	0.83	0.005431	1.9	0.03565	9.1	0.04761	8.9	0.21	34.9	0.7	35.6	3.2
a9	7552	807	4.7	0.97	0.15	0.005048	2.1	0.03226	6.3	0.04635	5.9	0.33	32.5	0.7	32.2	2.0
a10	8317	863	5.2	0.89	b.d.	0.005129	2.4	0.03522	20	0.04980	20	0.12	33.0	0.8	35.1	7.0
a11	6077	636	3.7	0.78	0.73	0.005161	2.3	0.03377	7.6	0.04745	7.2	0.31	33.2	0.8	33.7	2.5
a12	10597	1159	6.6	0.80	0.09	0.005141	2.0	0.03399	7.6	0.04795	7.4	0.26	33.1	0.7	33.9	2.6
a13	9291	961	5.8	0.99	b.d.	0.005178	2.0	0.03362	6.5	0.04709	6.2	0.31	33.3	0.7	33.6	2.2
a14	10839	1138	6.9	0.86	b.d.	0.005114	2.5	0.03200	6.8	0.04537	6.3	0.36	32.9	0.8	32.0	2.1
a15	10773	1067	6.5	0.93	b.d.	0.005154	2.1	0.03286	5.4	0.04624	5.0	0.38	33.1	0.7	32.8	1.8
a16	4655	473	2.7	0.76	b.d.	0.005130	2.2	0.03391	11	0.04794	10	0.21	33.0	0.7	33.9	3.5
a17	7796	791	4.6	0.84	b.d.	0.005118	2.3	0.03340	7.5	0.04733	7.1	0.31	32.9	0.8	33.4	2.5
a18	10606	1127	8.9	0.91	12.6	0.005010	2.8	0.03200	8.4	0.04633	8.0	0.33	32.2	0.9	32.0	2.7
a19	5670	591	3.4	0.78	b.d.	0.005111	2.4	0.03394	6.7	0.04816	6.2	0.36	32.9	0.8	33.9	2.2
a20	9456	1024	6.1	0.97	b.d.	0.005074	2.1	0.03240	5.3	0.04631	4.9	0.40	32.6	0.7	32.4	1.7
a21	7150	751	4.6	1.01	1.23	0.005164	1.9	0.03419	5.3	0.04803	4.9	0.37	33.2	0.6	34.1	1.8
a22	17449	1911	13	1.43	2.69	0.004978	2.0	0.03252	4.3	0.04739	3.9	0.46	32.0	0.6	32.5	1.4
a23	6173	645	3.8	0.78	1.84	0.005193	2.4	0.03316	9.8	0.04631	9.6	0.24	33.4	0.8	33.1	3.2
a24	6245	675	3.8	0.75	1.29	0.005006	2.6	0.03219	5.7	0.04664	5.1	0.46	32.2	0.8	32.2	1.8
a25	8590	936	5.7	0.91	0.56	0.005366	1.9	0.03514	7.9	0.04750	7.7	0.24	34.5	0.7	35.1	2.7
**a26	27331	355	19	0.62	6.06	0.04684	1.9	0.3382	3.4	0.05237	2.9	0.56	295	6	296	9
a27	12101	1302	8.3	0.85	1.81	0.005114	2.7	0.03420	6.5	0.04850	6.0	0.41	32.9	0.9	34.1	2.2
a28	3390	333	2.7	0.93	8.1	0.005163	3.7	0.03289	15	0.04620	14	0.25	33.2	1.2	32.9	4.7
a29	9297	981	6.1	0.63	3.61	0.005106	2.6	0.03228	8.5	0.04586	8.1	0.31	32.8	0.9	32.3	2.7
a30	11382	1247	9.2	1.14	3.79	0.005054	3.2	0.03498	5.5	0.05021	4.5	0.58	32.5	1.0	34.9	1.9

Spot size = 20 and 30 μm , respectively; depth of crater $\sim 20 \mu\text{m}$. $^{206}\text{Pb}/^{238}\text{U}$ error is the quadratic additions of the within run precision (2 SE) and the external reproducibility (2 SD) of the reference zircon. $^{207}\text{Pb}/^{206}\text{Pb}$ error propagation (^{207}Pb signal dependent) following Gerdes and Zeh (2006, 2009). $^{207}\text{Pb}/^{235}\text{U}$ error is the quadratic addition of the $^{207}\text{Pb}/^{206}\text{Pb}$ and $^{206}\text{Pb}/^{238}\text{U}$ uncertainty.

*Within run background-corrected mean ^{207}Pb signal in cps (counts per second).

$^\dagger\text{U}$ and Pb content and Th/U ratio were calculated relative to GJ-1 reference zircon.

‡ percentage of the common Pb on the ^{206}Pb . b.d. = below detection limit.

§ corrected for background, within-run Pb/U fractionation (in case of $^{206}\text{Pb}/^{238}\text{U}$) and common Pb using Stacey and Kramers (1975) model Pb composition and subsequently normalized to GJ-1 (ID-TIMS value/measured value); $^{207}\text{Pb}/^{235}\text{U}$ calculated using $^{207}\text{Pb}/^{206}\text{Pb}/(^{238}\text{U}/^{206}\text{Pb} * 1/137.88)$.

¶ Rho is the $^{206}\text{Pb}/^{238}\text{U}/^{207}\text{Pb}/^{235}\text{U}$ error correlation coefficient.

**Excluded from the calculation of average age.

1990). Biotite K–Ar ages from one of these sandstone beds are $32.0 \pm 2.8 \text{ Ma}$ and from below the Tard Fm. are $31.7 \pm 1.6 \text{ Ma}$ (Báldi *et al.*, 1981), which overlap with, or are slightly younger than, the stratigraphic age ($\sim 33 \text{ Ma}$ at 736 m, Fig. 2).

At 612 m the Tard Fm. is truncated by a terrestrial clastic sequence (upper NP23 or lower NP24 nannozone). From 506.8 to 180 m, the clastic sequence changes to marine siltstone and sandstone (NP24 and NP25), which suggests a marginal position in the basin. At

180 m, the Palaeogene strata are truncated; estimates for erosion vary between 100 m and 500 m based on analogy with other parts of the NPHB (Báldi, 1986). From 180 m, the overlying syn-rift sediments (siltstone, limestone, sandstone) of late Early Miocene age (17.3–16.5 Ma; Kókay, 1988) are overlain, after a hiatus at 16–12.8 Ma, by upper Middle Miocene limestone and gravel. No Upper Miocene–Lower Pliocene sediments are found in the borehole; however, a $\sim 300 \text{ m}$ thick sequence eroded during the latest Pliocene to Quaternary can be inferred from the

surrounding area. Present-day borehole temperatures indicate a geothermal gradient of $46 \text{ }^\circ\text{C km}^{-1}$.

Samples and methods

Six samples of volcanoclastic sediments were collected from depths of 640–800 m for geo-/thermochronological investigations (Fig. 2; Tables 1–3). Apatite was dated by fission track and (U–Th)/He methods, and zircon by U–Pb LA-ICP-MS. The low-temperature thermal history yielded by the thermochronological data was modelled using HeFTy

Table 2 Apatite fission track data for borehole AD-3.

Sample code	Stratigraphy	Lithology	Depth (m)	Depth							P(χ^2) (%)	Age (Ma)	$\pm 2\sigma$ (Ma)	MTL (μm)	SD (μm)	Dpar (μm)	SD (μm)		
				N	RhoS	N_s	Rhol	N_i	RhoD	N_d									
AD-3-1	Lower Oligocene	Volcanogenic sandstone	−643.2	25	1.630	286	4.183	734	7.119	3315	>95	0.00	43.4	6.4	15.2	1.3	57	3.9	0.2
AD-3-2	Lower Oligocene	Volcanogenic sandstone	−656.8	20	1.549	214	4.146	573	7.129	3315	>96	0.00	41.6	6.8	15.5	1.2	20	3.6	0.2
AD-3-3	Lower Oligocene	Volcanogenic sandstone	−669	20	1.226	198	3.287	531	7.140	3315	>97	0.00	41.6	7.2	16.3	1.1	35	4.0	0.3
AD-3-4	Lower Oligocene	Volcanogenic sandstone	−681.2	20	1.512	205	4.329	587	7.150	3315	>98	0.00	39.0	6.6	15.4	1.3	34	3.9	0.3
AD-3-5	Lower Oligocene	Volcanogenic sandstone	−698	20	1.393	194	3.921	546	7.161	3315	>99	0.00	39.8	6.8	15.7	1.1	12	3.8	0.1
AD-3-6	Upper Eocene	Volcanogenic sandstone	−802	25	1.834	328	5.933	1061	7.171	3315	84	0.01	34.7	4.6	14.6	1.1	36	3.7	0.2

N , number of dated apatite crystals; RhoS (Rhol), spontaneous (induced) track densities ($\times 10^5$ tracks cm^{-2}); N_s (N_i), number of counted spontaneous (induced) tracks; RhoD, dosimeter track density ($\times 10^5$ tracks cm^{-2}); N_d , number of tracks counted on dosimeter; P (χ^2), probability obtaining chi-squared value (χ^2) for n degrees of freedom (where $n = \text{No. of crystals} - 1$); Disp., dispersion; Age $\pm 1\sigma$, central age ± 2 standard error (Galbraith and Laslett, 1993); MTL, mean track length; SD, standard deviation; N (L), number of horizontal confined tracks measured; Dpar, average etch pit diameter of fission tracks (5 Dpars were measured per each dated grain).

Ages were calculated using zeta calibration method (Hurford and Green, 1983), glass dosimeter CN-5 and zeta value of 313.6 ± 3.7 year cm^{-2} .

(Ketcham, 2005). In addition, subsidence and thermal history from borehole stratigraphy, temperature and new vitrinite reflectance data (Table S1) were modelled with PetroMod 1D (Littke *et al.*, 1994; Hantschel and Kauerauf, 2009). Details of the analytical and modelling procedures can be found in Data S1.

Results and interpretation

Analytical results are summarized in Tables 1–3, Figs 2–3 and Table S1. Sample AD-3-3 (667 m) yielded a $^{206}\text{Pb}/^{238}\text{U}$ age of 32.72 ± 0.15 Ma (Fig. 4). We interpret this age as the crystallization age of the zircons, which preceded their eruption to the surface. This age is in excellent agreement with the biostratigraphic age of 32.9–29.7 Ma for the NP22-23 nannozones (Vandenberghe *et al.*, 2012) and biotite K–Ar ages of Báldi *et al.* (1981).

All apatites have large Dpars (>3.5 μm), indicating chlorine-rich composition and an elevated temperature range of the partial annealing zone at ~ 70 – 130 °C (Green *et al.*, 1989; Carlson *et al.*, 1999; Barbarand *et al.*, 2003). All AFT ages from the Oligocene strata (AD-3-1 to -5) cluster between 43.4 ± 6.4 and 39 ± 6.6 Ma. The deepest sample (AD-3-6; Upper Eocene) revealed an AFT age of 34.7 ± 4.6 Ma (Fig. 3). Long mean track

lengths (>14.6 μm) suggest an extremely fast cooling, characteristic of volcanic rocks (Gleadow *et al.*, 1986). Fast cooling is also corroborated by the ZFT age of 34.9 ± 6.6 Ma (Dunkl, 1990), which is almost identical to the AFT age (34.7 ± 4.6 Ma) from the same sample (AD-3-6). The AFT ages record volcanic eruptions during Lutetian-Bartonian and late Priabonian times, clearly older than the zircon U–Pb ages and the micropalaeontologically determined sedimentation ages. This indicates a complex provenance for the volcanic material, whereby the U–Pb dated zircon grains derived from syn-sedimentary eruptions while the apatites were re-deposited from an older volcanic source. The euhedral morphology of the apatites, without traces of abrasion, suggests transport over a short distance and, given the close proximity of the volcanic centre of the Velence Hills volcanism (~ 15 km SW from Ad-3), this is the most likely source area (Fig. 1a).

AHe ages of 23.8 ± 2.8 to 14.8 ± 2.2 Ma are significantly younger than the depositional age and the corresponding AFT ages, which points to a post-depositional thermal event that at least partially reset the (U–Th)/He system (Fig. 4).

Scatter of vitrinite reflectance values (0.23–0.40%) and high fluorescence intensity of liptinites indicate

low maturity and heterogeneity of the organic matter (Table S1).

Thermal trajectories modelled with HeFTy that reconcile AFT and AHe data suggest a heating to temperatures of ~ 65 – 80 °C, loosely constrained between ~ 24 and 11 Ma (Fig. 4). We note that this heating event did not cause any shortening of fission tracks in apatite owing to their high annealing resistivity given by their chlorine-rich composition. PetroMod-based modelling refined the timing of the thermal maximum to 17 Ma and suggests maximum temperatures of 58 – 66 °C in the Tard Fm. (Figs 4; S5–S10), which is in good agreement with the HeFTy estimate. Interpretation of the thermal event is discussed in Section ‘Implications for interpretation of AHe data’.

Discussion

Geodynamic implications

The Velence Hills volcanoes, located 10–20 km west of the western margin of the NHPB (Fig. 1a), were active during the Middle and Late Eocene as evidenced by biostratigraphy and K/Ar data (Fig. 2; Darida-Tichy and Horváth, 2004; Benedek, 2002; Ker-csmár *et al.*, 2008). The new AFT and published ZFT ages (Dunkl, 1990) corroborate this evidence. In the Early Oligocene, the volcanic

Table 3 Apatite (U-Th)/He data for borehole AD-3.

Sample code	Th (ng)	± (%)	U (ng)	± (%)	Sm (ng)	± (%)	He (ncc)	± (%)	TAU (%)	Th/U	Unc. age (Ma)	±2σ (Ma)	Ft	Cor. age (Ma)	±2σ (Ma)
AD-3-1															
a	0.172	2.4	0.035	5.5	0.3	5.9	0.098	1.0	5.2	4.84	10.7	1.1	0.73	14.8	2.1
b	0.209	2.4	0.055	3.6	0.6	5.8	0.207	0.9	5.1	3.74	16.3	1.7	0.76	21.4	3.1
c	0.300	2.4	0.055	3.6	0.5	5.5	0.217	0.9	4.7	5.38	14.2	1.3	0.76	18.6	2.5
d	0.271	2.4	0.069	3.0	0.9	5.5	0.246	0.9	4.9	3.92	15.3	1.5	0.78	19.6	2.7
e	0.231	2.4	0.062	3.4	0.7	5.5	0.234	0.9	4.9	3.72	16.5	1.6	0.77	21.3	3.0
f	0.148	2.4	0.035	5.0	0.4	5.8	0.108	1.0	5.2	4.21	12.7	1.3	0.73	17.4	2.5
Average age ± 2σ (both in Ma)														18.3	± 2.8
AD-3-2															
a	0.205	2.4	0.044	4.2	0.6	5.5	0.164	0.9	4.9	4.61	14.6	1.4	0.75	19.5	2.7
b	0.187	2.4	0.041	4.6	0.6	5.5	0.157	0.9	5.0	4.54	15.2	1.5	0.75	20.2	2.8
c	0.223	2.4	0.049	3.8	0.6	5.3	0.186	0.9	4.7	4.50	15.0	1.4	0.75	20.0	2.8
d	0.299	2.4	0.069	2.6	0.9	2.9	0.312	0.9	2.9	4.28	18.4	1.1	0.78	23.5	2.7
e	0.328	2.4	0.074	2.5	0.9	3.1	0.302	0.9	3.0	4.43	16.5	1.0	0.79	20.8	2.4
f	0.193	2.4	0.044	3.4	0.5	2.9	0.196	0.9	3.0	4.35	18.0	1.1	0.75	23.8	2.8
Average age ± 2σ (both in Ma)														21.3	± 1.9
AD-3-3															
a	0.301	2.4	0.083	2.3	1.0	2.9	0.330	0.9	2.9	3.60	17.6	1.0	0.79	22.2	2.6
b	0.183	2.4	0.041	3.6	0.6	2.8	0.137	0.9	2.9	4.43	13.4	0.8	0.76	17.6	2.0
c	0.375	2.4	0.095	2.2	1.2	2.6	0.333	0.9	2.7	3.91	14.9	0.8	0.81	18.3	2.1
d	0.332	2.4	0.080	2.4	1.1	2.7	0.354	0.9	2.8	4.13	18.4	1.0	0.81	22.8	2.6
e	0.210	2.4	0.055	2.9	0.7	3.5	0.169	0.9	3.4	3.76	13.3	0.9	0.77	17.3	2.1
f	0.131	2.4	0.031	4.4	0.4	2.8	0.104	0.9	3.0	4.23	13.8	0.8	0.71	19.3	2.3
Average age ± 2σ (both in Ma)														19.2	± 2.3
AD-3-4															
a	0.122	2.4	0.029	4.7	0.4	3.6	0.106	0.9	3.6	4.25	15.2	1.1	0.73	20.7	2.5
b	0.222	2.4	0.064	2.7	0.7	2.8	0.179	0.9	2.8	3.42	12.6	0.7	0.77	16.4	1.9
c	0.167	2.4	0.043	3.5	0.6	2.7	0.149	0.9	2.8	3.89	14.9	0.8	0.76	19.6	2.3
d	0.103	2.4	0.027	5.2	0.4	4.5	0.078	0.9	4.3	3.84	12.6	1.1	0.76	16.5	2.2
e	0.167	2.4	0.043	3.4	0.5	3.3	0.152	0.9	3.2	3.89	15.3	1.0	0.76	20.2	2.4
Average age ± 2σ (both in Ma)														18.3	± 2.6
AD-3-5															
a	0.334	2.4	0.097	2.2	1.5	2.9	0.396	1.1	3.0	3.43	18.5	1.1	0.81	22.8	2.7
b	0.240	2.4	0.071	2.5	1.4	2.6	0.236	1.1	2.8	3.34	15.2	0.8	0.80	19.1	2.2
c	0.247	2.4	0.052	3.1	1.1	2.8	0.194	1.1	3.0	4.74	14.5	0.9	0.79	18.4	2.1
d	0.373	2.4	0.079	2.4	1.5	2.5	0.374	1.1	2.7	4.67	18.4	1.0	0.82	22.5	2.6
e	0.199	2.4	0.040	3.5	0.8	3.5	0.154	1.2	3.5	4.90	14.5	1.0	0.73	19.9	2.4
Average age ± 2σ (both in Ma)														20.2	± 2.5
AD-3-6															
a	0.173	2.4	0.045	3.4	0.5	3.4	0.149	1.2	3.4	3.86	14.4	1.0	0.73	19.9	2.4
b	0.208	2.4	0.044	3.5	0.5	3.2	0.132	1.3	3.3	4.68	11.6	0.8	0.70	16.6	2.0
Average age ± 2σ (both in Ma)														18.0	± 1.5

Th, ^{232}Th ; U, ^{238}U ; Sm, ^{147}Sm ; He, ^4He ; TAU, total analytical uncertainty; Unc. age, uncorrected He age; Ft, alpha recoil correction factor after Farley *et al.* (1996); Cor. age, corrected He age. Average age for the population was calculated as error weighted average using Isoplot Excel Add-in (Ludwig, 2001); 2 sigma uncertainty is the error propagated from the assigned data-point errors multiplied by the square root of the MSWD and Student's-*t* for *N*-1 degrees of freedom.

centres experienced denudation, as documented by a hiatus in the TPB (Fig. 2; Telegdi Roth, 1927). Our data prove that the eroded volcanic material of the TPB was finally deposited in the western margin of the younger NHPB, in the Tard Fm. (Fig. 2). K/Ar ages suggest that volcanism in the Velence Hills likely continued in the Early Oligocene (Józsa, 1983; Benedek, 2002; Darida-Tichy and Horváth, 2004) as it did

in other volcanic centres in both Hungarian Palaeogene Basins (Fig. 1a; Dunkl and Nagymarosy, 1992; Benedek, 2002; Less *et al.*, 2009). The U–Pb dated zircon can be connected to any of these volcanic centres.

All Hungarian volcanic centres are close to the Mid-Hungarian Fault Zone, a continuation of the Periadriatic Fault system (PAF; Benedek, 2002; Bergomi *et al.*, 2015). Magma-

tism along the PAF included intrusions within the fault zone, variable sized plutons, subvolcanic bodies and dikes (Bergomi *et al.*, 2015) in the vicinity of the PAF (Fig. 1a). The temporal and spatial relationships suggest that the Hungarian volcanoes are related to subsurface Alpine magmatic bodies. The most extensively studied igneous centre of this belt is the Adamello Complex (e.g. Schoene *et al.*, 2012) where the evolution of

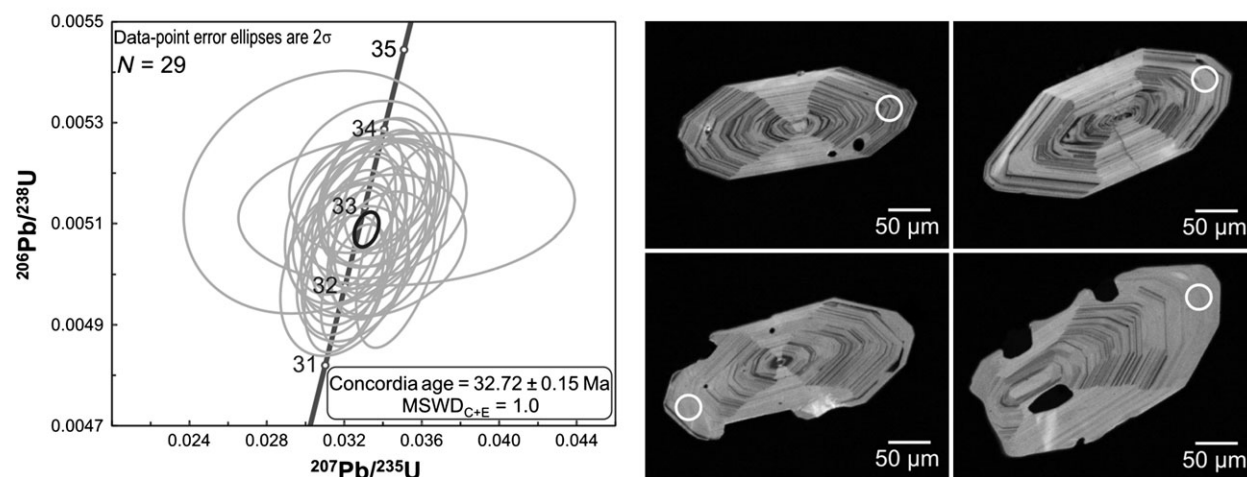


Fig. 3 Left: Zircon U–Pb concordia plot for sample AD-3-3 (667 m). Grey ellipses – 2σ uncertainties of single data-points; black ellipse – pooled concordia age of the 29 analyses with 2σ uncertainty. Right: Selected cathodoluminescence images with position of LA-ICP-MS spots (white circles), showing characteristic oscillatory zoning and in some cases resorbed character of the dated zircon crystals.

the igneous suite started with emplacement of mafic members (~42 Ma) and continued to more evolved, acidic magmas (~32 Ma). In this sequence, the accessory minerals were first dominated by apatite, and the abundance of zircon increased with time (Schoene *et al.*, 2012). We assume that this evolution is reflected in the mixed accessory minerals at the Ad-3 site: the 43 to 40 Ma apatites were derived from the first, more mafic magmatites, while the zircons (~33 Ma) originated from the more evolved acid magmatites.

Early Miocene AHe ages could be explained either by sedimentary burial of an Oligo-Miocene cover sequence or by an increasing heat flow. The first scenario assumes burial of the Lower Oligocene horizons by Neogene sediments of great thicknesses or low thermal conductivity, followed by exposure due to erosional denudation, and may find support in the Plio-Quaternary denudation reported in several parts of the Pannonian Basin (Dunkl and Frisch, 2002). We used PetroMod 1D to test various burial scenarios, including Late Oligocene–Early Miocene, mid-Miocene and Late Miocene overburden, using observed stratigraphical gaps (Fig. 2). When assuming plausible maximum burial thicknesses estimated from the regional stratigraphy, the modelled maxi-

mum temperatures were not sufficiently high to reset the AHe thermochronometer (Fig. 4b). Thus, the only way to reach the desired temperatures is an increased heat flow during the Miocene (Fig. 4; S5–S7). This is in agreement with the increased Miocene heat flow reported from other parts of the Pannonian Basin, which reached 100–120 mW m^{-2} during the syn-rift phase (Dövényi and Horváth, 1988; Sachsenhofer *et al.*, 1997; Sachsenhofer, 2001; Lenkey *et al.*, 2002) and is significantly higher than the present-day value (80–90 mW m^{-2}).

It has been shown that elevated heat flow in the Miocene was responsible for resetting AFT and AHe thermochronometers in other parts of the Pannonian Basin and in the neighbouring Western Carpathians (Danišik *et al.*, 2008, 2012). Its widespread regional character suggests that elevated heat flow was related to lithospheric thinning and asthenospheric diapir formation (Stegena *et al.*, 1975; Horváth and Royden, 1981; Dövényi and Horváth, 1988; Tari *et al.*, 1999), rather than to local magmatic activity. This is supported by the fact that there are no Miocene volcanic centres in the vicinity of the borehole (Fig. 1b). The Ad-3 borehole is located at the edge of a N–S trending syn-rift graben, where crustal thinning was important (Fig. 1b).

Implications for interpretation of AHe data

AHe dating has been extensively used to quantify exhumation and erosion rates using various approaches including the mineral pair method, elevation profiles, or the lag-time concept (e.g. Stock *et al.*, 2006; Rahl *et al.*, 2007; Glotzbach *et al.*, 2010). In the majority of studies, AHe ages are interpreted as cooling ages, i.e. ages recording apatite cooling through the closure isotherm or partial retention zone at the dated time, whereby the cooling rate is usually not known but is assumed to be high. This rather simplistic interpretation, based on the closure temperature concept (Dodson, 1973), is plausible and even realistic in some cases. However, the potential that a (U–Th)/He age is merely a number resulting from competing accumulation and diffusion of ^4He (cf. Wolf *et al.*, 1998), and does not necessarily represent a distinct geological event, should not be neglected. Given the sensitivity of the AHe system to low temperatures and the high likelihood of its opening by even subtle heating, the majority of rocks in nature should reveal ‘apparent’ AHe ages without direct geological meaning rather than ‘cooling ages’. Therefore, the term ‘apparent AHe age’ should be used in data interpretations and

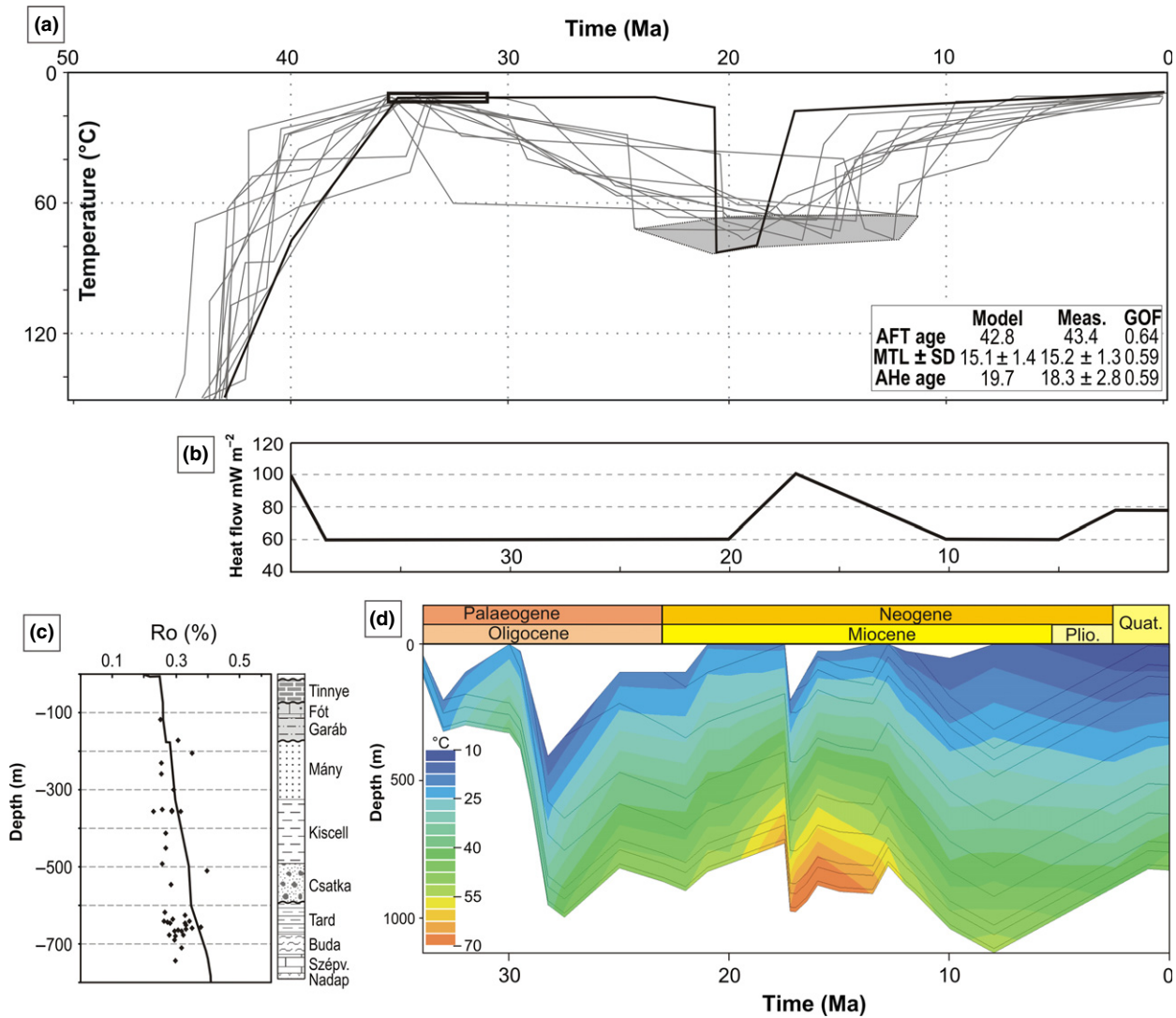


Fig. 4 (a) Thermal modelling results for sample AD-3-1 based on thermochronological data. The modelling was performed by HeFTy (Ketcham, 2005); the constraints were the age of volcanism (~42 Ma) and the age of sedimentation at ~32 Ma (rectangle). The grey area represents the time-temperature range of the climax of the thermal overprint. Grey curves – good fit thermal trajectories; thick black curve – best fit thermal trajectory. (b) Heat flow history for thermal modelling shown in Fig. D. For comparison with other heat flow histories see Figure S2. (c) Maturity–depth plot. Black line – modelled vitrinite reflectance; dots – measured vitrinite reflectance. Lithology of the formations is the same as in Fig. 2. For details and input data see Data S1. (d) Subsidence and thermal modelling of the sequence in Ad-3 for the scenario with a 17 Ma heat flow peak (PetroMod 1D software; Littke *et al.*, 1994; Hantschel and Kauerauf, 2009). Heat flow was kept at 60 mW m⁻², except for the periods of 20–10 Ma and 5–0 Ma, where there was a heat flow maximum of 100 mW m⁻² at 17 Ma, and an increase to 75 mW m⁻² respectively. Note the good agreement of the Miocene thermal maximum revealed by the two modelling approaches.

entrenched in (U–Th)/He terminology, as is the case in the fission track literature. It is obvious that a direct conversion of ‘apparent’ AHe ages into cooling, exhumation or erosion rates is incorrect.

This study highlights the importance of a multi-methodological

approach for dating volcanic rocks and presents potential pitfalls in the interpretation of AHe data. Without AFT, U–Pb or biostratigraphic data, AHe ages would be falsely interpreted as cooling or eruption ages. Availability of the aforementioned

data, in which AHe ages from volcanic rocks are neither cooling nor eruption ages, but apparent ages.

Conclusions

- The new zircon U–Pb age of 32.72 ± 0.15 Ma conclusively proves

Early Oligocene volcanism in the Hungarian Palaeogene Basins, and is in excellent agreement with the biostratigraphic age (NP22–23 zones) of the zircon-bearing sediment. This age is currently the most accurate tie-point for the correlation of the Early Oligocene volcanoclastic levels in the entire Pannonian Basin;

- The volcanoclastic sequence has a mixed character – the zircon crystals were derived from syn-sedimentary Early Oligocene eruptions, and the apatites (43.4 ± 6.4 to 39.0 ± 6.6 Ma) originated from re-deposition of an older, Eocene volcanic source, likely the Velence Hills. The dominance of older apatite-rich and younger zircon-rich igneous products shows a strong similarity to the evolution of the Adamello Complex;
- Apatite (U–Th)/He ages of 23.8 ± 2.8 to 14.8 ± 2.2 are considerably younger than the age of sedimentation. Thermal modelling that considers AFT, AHe and vitrinite reflectance data lends credit to a period of increased heat flow at ~ 17 Ma, which coincides with the main rifting phase in the Pannonian basin, and therefore is attributed to mantle upwelling;
- The common practice of interpreting (U–Th)/He ages as ‘cooling’ ages (i.e. ages of a distinct cooling event) and their translation into exhumation, erosion or denudation rates may be erroneous even in the simplest cases such as the dating of volcanic rocks. Thus, we recommend applying a multi-methodical approach involving other thermo-/geochronometers, thermal maturity data and/or stratigraphy to reconstruct a robust thermal history from (U–Th)/He data, especially in the case of mixed volcanoclastic formations.

Acknowledgement

The study was supported by the Hungarian Scientific Research Found No. 42799 and Austrian-Hungarian Action Foundation No 680u7. Part of the stratigraphical column was drawn by Z. Lantos (Budapest), and O. Sztanó (Budapest) contributed to sedimentological interpretation. Finally, we thank an anonymous reviewer, C. Persano, F. Horváth, and the

associate editor Meinert Rahn for detailed and constructive reviews.

References

- Bachmann, O., Oberli, F., Dungan, M.A., Meier, M., Mundil, R. and Fischer, H., 2007. Ar-40/Ar-39 and U-Pb dating of the Fish Canyon magmatic system, San Juan Volcanic field, Colorado: evidence for an extended crystallization history. *Chem. Geol.*, **236**, 134–166.
- Báldi, T., 1986. *Mid-Tertiary Stratigraphy and Paleogeographic Evolution of Hungary*. Akadémia Press, Budapest. 293 pp.
- Báldi, T., Horváth, M., Nagymarosy, A. and Varga, P., 1981. Jelentés a 3329/80 sz. állami megbízás kutatómunkáról. A kiscelli emelet alapszelvényeinek vizsgálata és értékelése. Manuscript, Archive of the Geological and Geophysical Institute of Hungary, in Hungarian, 270 pp.
- Báldi, T., Horváth, M., Nagymarosy, A. and Varga, P., 1984. The Eocene-Oligocene boundary in Hungary. The Kiscellian Stage. *Acta Geol. Hung.*, **27**, 41–65.
- Barbarand, J., Carter, A., Hurford, T. and Wood, I., 2003. Compositional and structural control of fission-track annealing in apatite. *Chem. Geol.*, **198**, 107–137.
- Bechtel, A., Hámor-Vidó, M., Gratzler, R., Sachsenhofer, R.F. and Püttmann, W., 2012. Facies evolution and stratigraphic correlation in the early Oligocene Tard Clay of Hungary as revealed by maceral, biomarker and stable isotope composition. *Mar. Petrol. Geol.*, **35**, 55–74.
- Benedek, K., 2002. Paleogene igneous activity along the easternmost segment of the Periadriatic-Balaton Lineament. *Acta Geol. Hung.*, **45**, 359–371.
- Benedek, K., Pécskay, Z., Szabó, C., Jósvai, J. and Németh, T., 2004. Paleogene igneous rocks in the Zala Basin (Western Hungary): link to the Paleogene magmatic activity along the Periadriatic Lineament. *Geol. Carpath.*, **55**, 43–50.
- Bergomi, M.A., Zanchetta, S. and Tunesi, A., 2015. The Tertiary dike magmatism in the Southern Alps: geochronological data and geodynamic significance. *Int. J. Earth Sci.*, **104**, 449–473.
- Brandon, M.T., Roden-Tice, M.K. and Garver, J.I., 1998. Late Cenozoic exhumation of the Cascadia accretionary wedge in the Olympic Mountains, NW Washington State. *GSA Bull.*, **110**, 985–1009.
- Carlson, W.D., Donelick, R.A. and Ketcham, R.A., 1999. Variability of apatite fission-track annealing kinetics: I. Experimental results. *Am. Mineral.*, **84**, 1213–1223.
- Chen, Y., Smith, P.E., Evensen, N.M., York, D. and Lajoie, K.R., 1996. The edge of time: dating young volcanic ash layers with the $^{40}\text{Ar}/^{39}\text{Ar}$ laser probe. *Science*, **274**, 1176–1178.
- Csontos, L. and Nagymarosy, A., 1998. The Mid-Hungarian line: a zone of repeated tectonic inversion. *Tectonophysics*, **297**, 51–72.
- Danišik, M., Kohút, M., Dunkl, I., Hraško, L. and Frisch, W., 2008. Apatite fission track and (U–Th)/He thermochronology of the Rochovce granite (Slovakia) – implications for the thermal evolution of the Western Carpathian-Pannonian region. *Swiss J. Geosci.*, **101**, 225–233.
- Danišik, M., Kohút, M., Evans, N.J. and McDonald, B.J., 2012. Eo-Alpine metamorphism and the ‘mid-Miocene thermal event’ in the Western Carpathians (Slovakia): new evidence from multiple thermochronology. *Geol. Mag.*, **149**, 158–171.
- Darida-Tichy, M. and Horváth, I., 2004. Middle-Upper Eocene - Nadap Andesite Formation. In: *Geology of the Velence Hills and the Balatonfő. Explanatory Book of the Geological map of the Velence Hills (1:25000) and the Geological map of Pre-Sarmatian Surface of the Balatonfő-Velence Area (1:100000)* (L. Gyalog and I. Horváth, eds), pp. 45–59. Geological Institute of Hungary, Budapest.
- Davies, G.R., Halliday, A.N., Mahood, G.A. and Hall, C.M., 1994. Isotopic constraints on the production rates, crystallisation histories and residence times of pre-caldera silicic magmas, Long Valley, California. *Earth Planet. Sci. Lett.*, **125**, 17–37.
- Dodson, M.H., 1973. Closure temperatures in cooling geochronological and petrological systems. *Contrib. Mineral. Petrol.*, **40**, 259–274.
- Dövényi, P. and Horváth, F., 1988. A review of temperature, thermal conductivity, and heat flow data for the Pannonian basin. In: *The Pannonian Basin* (L.H. Royden and F. Horváth, eds). *AAPG Mem.*, **45**, 195–233.
- Dunkl, I., 1990. Fission track dating of tuffaceous Eocene formations of the North Bakony Mountains (Transdanubia, Hungary). *Acta Geol. Hung.*, **33**, 13–30.
- Dunkl, I. and Frisch, W., 2002. Thermochronologic constraints on the Late Cenozoic exhumation along the Alpine and West Carpathian margins of the Pannonian basin. In: *Neotectonics and Surface Processes: The Pannonian Basin and Alpine/Carpathian System* (S.A.P.L. Cloetingh, F.

- Horváth, G. Bada and A.C. Lankreier, eds). *EGU Stephan Mueller Spec. Publ. Ser.*, **3**, 120–134.
- Dunkl, I. and Nagymarosy, A., 1992. A new tie-point candidate for the Paleogene timescale calibration: Fission track dating of tuff layers of Lower Oligocene Tard Clay (Hungary). *Neues Jb. Geol. Paläontol. Abh.*, **186**, 345–364.
- Farley, K.A., 2002. (U-Th)/He dating: techniques, calibrations, and applications. *Rev. Mineral. Geochem.*, **47**, 819–844.
- Farley, K.A., Wolf, R.A. and Silver, L.T., 1996. The effect of long alpha stopping distances on (U-Th)/He ages. *Geochim. Cosmochim. Acta*, **60**, 4223–4229.
- Farley, K.A., Kohn, B.P. and Pillans, B., 2002. The effects of secular disequilibrium on (U-Th)/He systematics and dating of Quaternary volcanic zircon and apatite. *Earth Planet. Sci. Lett.*, **201**, 117–125.
- Fodor, L. and Kövér, Sz., 2013. Post-conference excursion: Cenozoic deformation of the northern Transdanubian Range (Vértes Hills). *Acta Mineral. Petrogr.*, Field guide series, **31**, 35–52.
- Fodor, L., Magyari, Á., Kázmér, M. and Fogarasi, A., 1992. Gravity-flow dominated sedimentation on the Buda paleoslope (Hungary) - record of Late Eocene continental escape of the Bakony unit. *Geol. Rundsch.*, **81**, 695–716.
- Fodor, L., Jelen, B., Márton, E., Skaberne, D., Čar, J. and Vrabec, M., 1998. Miocene-Pliocene tectonic evolution of the Slovenian Periadriatic Line and surrounding area – implication for Alpine-Carpathian extrusion models. *Tectonics*, **17**, 690–709.
- Galbraith, R.F. and Laslett, G.M., 1993. Statistical models for mixed fission track ages. *Nucl. Tracks Rad. Meas.*, **21**, 459–470.
- Gerdes, A. and Zeh, A., 2006. Combined U-Pb and Hf isotope LA-(MC)-ICP-MS analyses of detrital zircons: comparison with SHRIMP and new constraints for the provenance and age of an Armorican metasediment in Central Germany. *Earth Planet. Sci. Lett.*, **249**, 47–62.
- Gerdes, A. and Zeh, A., 2009. Zircon formation versus zircon alteration - new insights from combined U-Pb and Lu-Hf in-situ LA-ICP-MS analyses, and consequences for the interpretation of Archean zircon from the Central Zone of the Limpopo Belt. *Chem. Geol.*, **261**, 230–243.
- Gleadow, A.J.W., Duddy, I.R. and Green, P.F., 1986. Confined fission track lengths in apatite: a diagnostic tool for thermal history analysis. *Contrib. Mineral. Petrol.*, **94**, 405–415.
- Glotzbach, C., Reinecker, J., Danišik, M., Rahn, M., Frisch, W. and Spiegel, C., 2010. Thermal history of the central Gotthard and Aar massifs, European Alps: evidence for steady state, long-term exhumation. *J. Geophys. Res.*, **115**, F03017.
- Green, P.F., Duddy, I.R., Laslett, G.M., Hegarty, K.A., Gleadow, A.J.W. and Lovering, J.R., 1989. Thermal annealing of fission tracks in apatite. 4. Quantitative modeling techniques and extension to geological timescales. *Chem. Geol.*, **79**, 155–182.
- Hámorné Vidó, M., Zilahi Sebess, L. and Fodor, L., 2008. Oligocén öszlet süllyedéstörténete a Vértes Hegységben, ÉNy-Magyarországon. A 68öü7 számú OMAA projekt 2008. évi zárójelentése. Manuscript, Archive of the Geological and Geophysical Institute of Hungary, Budapest, 14 pp, in Hungarian.
- Hantschel, T. and Kauerauf, A.I., 2009. *Fundamentals of Basin and Petroleum Systems Modeling*. Springer, Berlin.
- Harangi, S., 2001. Neogene to Quaternary volcanism of the Carpathian-Pannonian Region - a review. *Acta Geol. Hung.*, **44**, 223–258.
- Horváth, F. and Royden, L., 1981. Mechanism for the formation of the intra-Carpathian basins: a review. *Earth Evol. Sci.*, **1**, 307–316.
- Hurford, A.J. and Green, P.F., 1983. The zeta age calibration of fission track dating. *Chem. Geol.*, **41**, 285–317.
- Józsa, S., 1983. Petrographic and geochemical study of andesite from the Velence Mts., Hungary. Unpublished MSc thesis, Eötvös University, Department of Petrography and Geochemistry, Budapest, 107 pp.
- Kázmér, M., Dunkl, I., Frisch, W., Kuhlemann, J. and Ozsvárt, P., 2003. The Palaeogene forearc basin of the Eastern Alps and Western Carpathians: subduction erosion and basin evolution. *J. Geol. Soc. London*, **160**, 413–428.
- Kercsmár, Z., Pálfalvy, S., Less, G., Kordos, L. and Budai, T., 2008. Eocene. In: *Geology of the Vértes Hills. Explanatory Book to the Geological Map of the Vértes Hills (1:50000)* (T. Budai and L. Fodor, eds), pp. 58–80. Geological Institute of Hungary, Budapest.
- Ketcham, R.A., 2005. Forward and inverse modeling of low-temperature thermochronometry data. In: *Low-Temperature Thermochronology: Techniques, Interpretations, and Applications* (P.W. Reiners and T.A. Ehlers, eds). *Rev. Mineral. Geochem.*, **58**, 275–314.
- Kóky, J., 1988. Marine Karpatian beds at Alcsútdoboz. Annual Report of the Hungarian Geological Institute of 1986, 263–279.
- Lenkey, L., Dövényi, P., Horváth, F. and Cloetingh, S.A.P.L., 2002. Geothermics of the Pannonian basin and its bearing on the neotectonics. In: *Neotectonics and Surface Processes: The Pannonian Basin and Alpine/Carpathian System* (S.A.P.L. Cloetingh, F. Horváth, G. Bada and A.C. Lankreier, eds). *EGU Stephan Mueller Spec. Publ. Ser.*, **3**, 29–40.
- Less, G., Báldi-Beke, M., Benedek, K., Fodor, L., Földessy, J., Pálfalvi, S. and Zelenka, T., 2009. Age revision – and paleogeographic significance of the Reck volcano (NE Hungary). 7th Meeting of the Central European Tectonic Studies Group (CETeG), Pécs, 21.
- Littke, R., Büker, C., Lückge, A., Sachsenhofer, R.F. and Welte, D.H., 1994. A new evaluation of paleo-heat flows and eroded thicknesses for the Carboniferous Ruhr Basin, western Germany. *Int. J. Coal Geol.*, **26**, 155–183.
- Lowe, D., 2011. Tephrochronology and its application: a review. *Quat. Geochron.*, **6**, 107–153.
- Ludwig, K.R., 2001. Users manual for Isoplot/Ex rev. 2.49. *Berkeley Geochronol. Centre Spec. Publ.*, **1a**, 56.
- McDougall, I. and Harrison, T.M., 1998. *Geochronology and Thermochronology by the ⁴⁰Ar/³⁹Ar Method*. Clarendon Press, Oxford, UK.
- Nagymarosy, A., 1990. Paleogeographical and paleotectonical outlines of some Intra-Carpathian Paleogene basins. *Geol. Zbornik – Geol. Carpath.*, **41**, 259–274.
- Palotai, M. and Csontos, L., 2010. Strike-slip reactivation of a Paleogene to Miocene fold and thrust belt along the central part of the Mid-Hungarian Shear Zone. *Geol. Carpath.*, **61**, 483–493.
- Pomella, H., Klötzli, U., Scholger, R., Stipp, M. and Fügenschuh, B., 2011. The Northern Giudicarie and the Meran-Mauls fault (Alps, Northern Italy) in the light of new paleomagnetic and geochronological data from boudinaged Eo-/Oligocene tonalites. *Int. J. Earth Sci.*, **100**, 1827–1850.
- Rahl, J.M., Ehlers, T.A. and van der Pluijm, B.A., 2007. Quantifying transient erosion of orogens with detrital thermochronology from syntectonic basin deposits. *Earth Planet. Sci. Lett.*, **256**, 147–161.
- Reimer, P.J., Baillie, M.G.L., Bard, E., Bayliss, A., Beck, J.W., Blackwell, P.G., Bronk Ramsey, C., Buck, C.E., Burr, G.S., Edwards, R.L., Friedrich, M., Grootes, P.M., Guilderson, T.P., Hajdas, I., Heaton, T.J., Hogg, A.G., Hughen, K.A., Kaiser, K.F., Kromer,

- B., McCormac, F.G., Manning, S.W., Reimer, R.W., Richards, D.A., Southon, J.R., Talamo, S., Turney, C.S.M., van der Plicht, J. and Weyhenmeyer, C.E., 2009. IntCal09 and Marine09 radiocarbon age calibration curves, 0–50,000 years cal BP. *Radiocarbon*, **51**, 1111–1150.
- Reiners, P.W., Spell, T.L., Nicolescu, S. and Zanetti, K.A., 2004. Zircon (U-Th)/He thermochronometry: He diffusion and comparisons with $^{40}\text{Ar}/^{39}\text{Ar}$ dating. *Geochim. Cosmochim. Acta*, **68**, 1857–1887.
- Royden, L.H., Horváth, F., Nagymarosy, A. and Stegena, F., 1983. Evolution of the Pannonian Basin System. 2. Subsidence and thermal history. *Tectonics*, **2**, 91–137.
- Sachsenhofer, R.F., 2001. Syn- and post-collisional heat flow in the Cenozoic Eastern Alps. *Int. J. Earth Sci.*, **90**, 579–592.
- Sachsenhofer, R.F., Lankreijer, A., Cloetingh, S. and Ebner, F., 1997. Subsidence analysis and quantitative basin modelling in the Styrian Basin (Pannonian Basin system, Austria). *Tectonophysics*, **272**, 175–196.
- Schmitt, A.K., Danišik, M., Evans, N.J., Siebel, W., Kiemele, E., Aydin, F. and Harvey, J.C., 2011. Acigöl rhyolite field, Central Anatolia (part 1): high-resolution dating of pre-eruptive zircon residence and rhyolite eruption episodes. *Contrib. Mineral. Petrol.*, **162**, 1215–1231.
- Schoene, B., Schaltegger, U., Brack, P., Lattkoczy, C., Stracke, A. and Günther, D., 2012. Rates of magma differentiation and emplacement in a ballooning pluton recorded by U-Pb TIMS-TEA, Adamello batholith, Italy. *Earth Planet. Sci. Lett.*, **355–356**, 162–173.
- Seward, D., 1974. Age of New Zealand Pleistocene substages by fission-track dating of glass shards from tephra horizons. *Earth Planet. Sci. Lett.*, **24**, 242–248.
- Siebel, W., Schmitt, A.K., Danišik, M., Chen, F., Meier, S., Weiß, S. and Eroğlu, S., 2009. Prolonged mantle residence of zircons xenocrysts from the western Eger rift. *Nat. Geosci.*, **2**, 886–890. doi:10.1038/NNGEO695.
- Stacey, J.S. and Kramers, J.D., 1975. Approximation of Terrestrial Lead Isotope Evolution by a 2-Stage Model. *Earth Planet. Sci. Lett.*, **26**, 207–221.
- Steininger, F., Müller, C. and Rögl, F., 1988. Correlation of Central Paratethys, Eastern Paratethys, and Mediterranean Neogene stages. In: *The Pannonian Basin* (L.H. Royden and F. Horváth, eds.). *AAPG Mem.*, **45**, 79–87.
- Stegen, L., Géczy, B. and Horváth, F., 1975. Late Cenozoic evolution of the Pannonian basin. *Tectonophysics*, **26**, 71–90.
- Stock, G.M., Ehlers, T.A. and Farley, K.A., 2006. Where does sediment come from? Quantifying catchment erosion with detrital apatite (U-Th)/He thermochronometry. *Geology*, **34**, 725–728.
- Tari, G., Báldi, T. and Báldi-Beke, M., 1993. Paleogene retroarc flexural basin beneath the Neogene Pannonian Basin: a geodynamical model. *Tectonophysics*, **226**, 433–455.
- Tari, G., Dövényi, P., Dunkl, I., Horváth, F., Lenkey, L., Stefanescu, M., Szafián, P. and Tóth, T., 1999. Lithospheric structure of the Pannonian basin derived from seismic, gravity and geothermal data. In: *The Mediterranean Basins: Tertiary Extension Within the Alpine Orogen* (B. Durand, L. Jolivet, F. Horváth and M. Séranne, eds). *Geol. Soc. London. Spec. Publ.*, **156**, 215–250.
- Telegdi Roth, K., 1927. Spuren einer infraoligozänen Denudation am norwestlichen Rande des Transdanubischen Mittelgebirges. *Földtani Közlöny*, **57**, 117–128.
- Vandenbergh, N., Hilgren, F. J. and Speijer, R.P., 2012. The Paleogene Period. In: *The Geologic Time Scale 2012* (F.M. Gradstein, J.G. Ogg, M.D. Schmitz and G.M. Ogg, eds), pp. 855–922. Elsevier, Boston, USA.
- Wagner, G.A. and Van den haute, P., 1992. *Fission-Track Dating*. Enke Verlag, Stuttgart.
- Wolf, R.A., Farley, K.A. and Kass, D.M., 1998. Modeling of the temperature sensitivity of the apatite (U-Th)/He thermochronometer. *Chem. Geol.*, **148**, 105–114.

Received 5 November 2014; revised version accepted 18 April 2015

Supporting Information

Additional Supporting Information may be found in the online version of this article:

Figure S1. Variation in vitrinite reflectance data with depth in the Ad-3 borehole (partly after Hámorné Vidó *et al.* 2008).

Figure S2. Supposed changes of the palaeo water depth for the Ad-3 borehole.

Figure S3. The present day heat flow calibration.

Figure S4. The applied heat flow models. Colours correspond to three possible models with heat flow maximum at major geodynamic events of the Pannonian Basin system.

Figure S5. Modelling results corresponding to scenario with 40–30 Ma heat flow peak and maximum erosion. Left side: Subsidence history with temperature overlay. Right side: Maturity depth plot. Black line – modelled vitrinite reflectance, crosses – measured vitrinite reflectance. See Table 1 for preserved and eroded stratigraphy and Figure 2 for heat flow history.

Figure S6. Modelling results corresponding to scenario with 17 Ma heat flow peak and maximum erosion. Left side: Subsidence history with temperature overlay. Right side: Maturity depth plot. Black line – modelled vitrinite reflectance, dots – measured vitrinite reflectance. See Table 1 for preserved and eroded stratigraphy and Figure 2 for heat flow history.

Figure S7. Modelling results corresponding to scenario with 10 Ma heat flow peak and maximum erosion. Left side: Subsidence history with temperature overlay. Right side: Maturity depth plot. Black line – modelled vitrinite reflectance, dots – measured vitrinite reflectance. See Table 1 for preserved and eroded stratigraphy and Figure 2 for heat flow history.

Figure S8. Modelling results corresponding to minimum erosion scenario and heat flow peak at 40–30 Ma. Left side: Subsidence history with temperature overlay. Right side: Maturity depth plot. Black line – modelled vitrinite reflectance, dots – measured vitrinite reflectance. See Table 2 for preserved and eroded stratigraphy and Figure 2 for heat flow history.

Figure S9. Modelling results corresponding to minimum erosion scenario and heat flow peak at 17 Ma. Left side: Subsidence history with temperature overlay. Right side: Maturity depth plot. Black line – modelled vitrinite reflectance, dots – measured vitrinite reflectance. See Table 2 for preserved and eroded stratigraphy and Figure 2 for heat flow history.

Figure S10. Modelling results corresponding to minimum erosion scenario and heat flow peak at 10 Ma. Left side: Subsidence history with temperature overlay. Right side: Maturity depth plot. Black line – modelled vitrinite reflectance,

dots – measured vitrinite reflectance. See Table 2 for preserved and eroded stratigraphy and Figure 2 for heat flow history.

Table S1. Vitrinite reflectance data.

Table S2. The modelled Palaeogene–Neogene sequence of the Ad-3 well with maximum erosion scenario.

Table S3. The modelled Palaeogene–Neogene sequence of the Ad-3

well with minimum erosion scenario.

Data S1. Analytical methods and modelling procedures.